International Journal of Rock Mechanics & Mining Sciences 78 (2015) 99–107

Contents lists available at ScienceDirect

International Journal of Rock Mechanics & Mining Sciences

journal homepage: www.elsevier.com/locate/ijrmms

Technical Note

A creep model for weakly consolidated porous sandstone including volumetric creep

Hong Zheng, Xia-Ting Feng*, Xian-jie Hao

State Key Laboratory for Geomechanics and Geotechnical Engineering, Institute of Rock and Soil Mechanics, Chinese Academy of Sciences, Wuhan 430071, China

ARTICLE INFO

Article history:
Received 11 November 2014
Received in revised form
2 April 2015
Accepted 19 April 2015

Keywords:
Visco-elastic
Time-dependant compaction
Porous sandstone
Creep model

1. Introduction

The mechanical properties of porous rock are quite different from that of comparatively well-compacted rocks due to the larger porosity.[1,2] For porous sandstone, a critical value of confining pressure is proved to exist during the process from mainly pressure-shear failure to mainly slough failure.[3] When the confining pressure is increased, the main pressure-shear failure can be changed into slough failure. For porous chalk, the failure of the sample is a result of the complete destruction of the pore structure; the cohesive chalk is transformed, after significant volumetric deformation, into a compacted powder.[4] The basic mechanical behaviour of porous rock involving its failure mechanism and deformation are strongly affected by the spherical or hydrostatic stress tensor. The rock skeleton used in reservoir engineering (e.g. during oil extraction and CO_2 disposal) is a porous layer. During the injection or extraction of pore fluid into or out from the reservoir, the effective stress field of the reservoir is varied with the changes in its pore pressure. The various stress fields influence the porous layer in the form of short and long-term deformation, which gives rise to the reduction of porosity and permeability and subsidence.[5–7] CO_2 injection and petroleum production operating independently can result in significant over- or under pressuring in a basin, potentially causing land uplift/subsidence.[8] The compaction of porous sandstone is driven by the effective stress, as well as the cementation and intergranular pressure solution. And the mechanical compaction is attributed to porosity, compressive property of the mineral and cementation, while the pressure solution compaction depends on the grain contact dissolution in pore fluid.[9] For weakly consolidated rock, time-dependant compaction under constant stress conditions is referred to as compaction creep controlled by grain failure and debonding due to slow (sub-critical) crack growth, as well as stress-induced dissolution–precipitation processes or intergranular pressure solution.[10] Therefore, research into the time-dependant deformation of a porous layer, such as porous sandstone, is of theoretical significance and practical value for the assessment of the stability of an underground cavity and subsidence prediction around reservoirs.

As a porous material, a reservoir consists of a rock skeleton and the pore fluid. The mechanical behaviour of the reservoir is significantly dependant on the rock skeleton. This paper mainly discusses the mechanical mechanism for the time-dependant deformation of porous rock as reservoir skeleton. When the pore pressure in the reservoir is gradually depleted, e.g. gas or oil production, groundwater exploitation[11–13], the underlying strata is developed into weakly consolidated layer due to the increasing effective stress. This research proposes a constitutive model to describe the time-dependant deformation of porous sandstone which is weakly consolidated. Various research studies have been conducted to the creep constitutive model of geologic material in three methods: empiricism[14,15], the thermodynamic framework[16–18] and the element model.[19,20] Compared with other methods, the

* Corresponding author.
E-mail addresses: xtfeng@whrsm.ac.cn, xia.ting.feng@gmail.com (X.-T. Feng).

http://dx.doi.org/10.1016/j.ijrmms.2015.04.021
1365-1609/

creep element model is more easy for numerical simulation and engineering application. The creep element model is consisted of elastic elements, plastic elements, and viscosity elements. Various combinations of these four basic elements form different models to represent different creep characteristics, e.g. Burgers model and Cvisc model.[21,22]

Different from comparatively well-compacted rocks, and attributed to its porosity, weakly compacted sandstone displays different deformation characteristics. For porous rock, two deformation mechanisms can be identified: volumetric deformation and shear deformation. The former is due to the swell-shrink characteristics of the pore structure under hydrostatic stress which cause collapse[23] and the expansion of pores or coalescence of adjacent pores. The latter is attributed to the distortion of the pores and rock matrix under deviatoric stress which may influence the connectivity of the pore structure. Furthermore, the change of pore fluid pressure influences the effective stress field in the rock skeleton that may induce a readjustment of the reservoir deformation field which had stabilised over geological time. Since the effective stress is always changing during the reservoir engineering operations, both short-term and long-term deformation should be considered for the porous rock in question.

This research investigated the creep behaviour of porous sandstone acting as a reservoir material. The scanning electron microscope (SEM) and mercury intrusion porosimetry (MIP) have been applied to investigate the basic physical properties of porous sandstone. Triaxial compressive tests were conducted to obtain the strength parameters of this porous sandstone. Creep tests under different stress levels were implemented to deduce its time-dependant deformation under different stress regimes. On the basis of the Burgers model, the volumetric viscosity element was proposed by considering the influence of hydrostatic stress components on viscous strain. This new constitutive model was established to describe the creep behaviour of porous sandstone. Furthermore, a numerical code was applied in the simulation of the time-dependant deformation behaviour of porous sandstone.

2. Experimental methods

Three types of laboratory test were used to investigate the physico-mechanical properties of porous sandstone. The first involved SEM examination and MIP to evaluate the physical properties of porous sandstone. This reflected the pore structure including the pore size distribution and pore connectivity. Secondly, triaxial compressive tests of porous sandstone specimens provided compressive strengths to determine the axial load applied during creep testing. Thirdly, triaxial creep tests were conducted to investigate the time-dependant deformation properties of the samples.

2.1. Basic physical properties of porous sandstone

The sandstone specimens used in these three tests were sampled from the same location and had similar physical properties. Porous sandstone is mainly composed of quartz, feldspar, silt and detritus cemented by clay minerals, calcite, limonite, etc. To observe the microstructure of the pore network in sandstone, the SEM was used: micrographs at 50 × and 500 × magnification are shown in Fig. 1(a) and (b), respectively.

Fig. 1(a) and (b) shows that the sandstone skeleton was a cementation of mineral particles with uneven grain sizes uneven. The sandstone grains had a high sphericity and perfect connectivity between internal pores.

According to the International Society for Rock Mechanics (ISRM), suggested methods for porosity/density determination using saturation and calliper techniques, the porosity of porous sandstone is measured as 22.15% and the dry density of porous sandstone is 2.17 g/cm^3. With the application of MIP, the pore size distribution diagram, in differential form, is as shown in Fig. 2. The abscissa represents the logarithm of pore size (in nanometres) and the ordinate represents the derivative of pore volume with respect to the logarithm of pore size (in cc/g). The pore size distribution diagram reflects the concentration of pore sizes. In Fig. 2, the logarithm of the pore size for porous sandstone was approximately 4 and the peak pore size was 8363 nm.

2.2. Compressive strength of porous sandstone

The specimens were prepared according to the ISRM suggested methods for triaxial compressive tests before drying at 45 °C for 48 h. To reduce error in the measurement of the physico-mechanical properties, specimens having wave velocities in the range of ±5% of the average were accepted. The cylindrical samples were 50 mm in diameter and 100 mm in tall.

A set of triaxial compression tests with confining pressure from 5 to 30 MPa were undertaken on three samples for each confining pressure. The temperature was set to a constant 25 °C. For each triaxial compression test, the cylindrical sample is firstly subjected to the confining pressure around the cylinder and top and bottom surface, i.e. the hydrostatic pressure state. Then the deviatoric stress is exerted in the cylinder axial direction on the top and

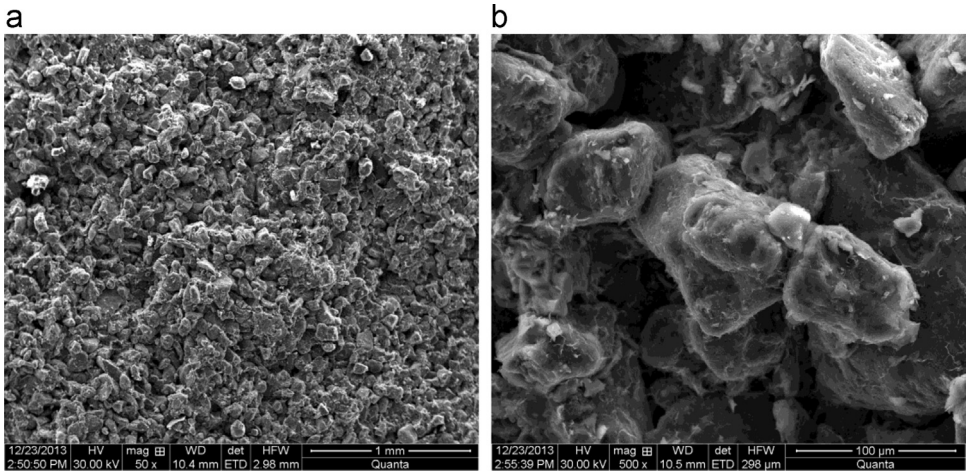

Fig. 1. SEM images at (a) 50 × magnification and (b) 500 × magnification: porous sandstone specimen.

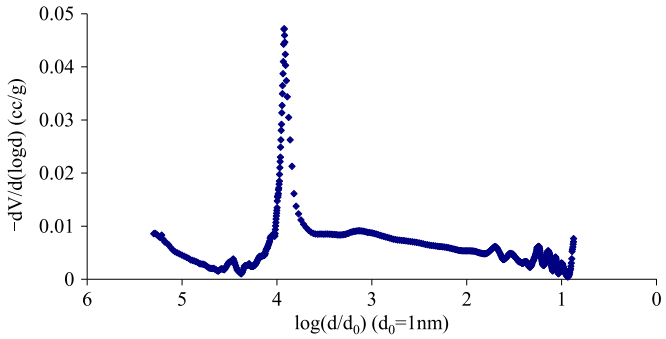

Fig. 2. Pore size distribution (in differential form) of porous sandstone.

bottom surface at the constant deformation rate of 10^{-6} m/s. Therefore, during the loading process, the maximum principal stress is the sum of confining pressure and deviatoric stress while the minimum principal stress and intermediate principal stress are both equal to the confining pressure. The compressive strength is figured out by adding the peak value of deviatoric stress to the confining pressure. And the compressive strength of porous sandstone samples under different confining pressures is listed in Table 1. These compressive strength data provided a reference for stress levels in subsequent creep tests.

2.3. Long-term deformation of porous sandstone

Different rock types have different creep patterns.[24] Porous sandstone, as a soft rock with the relatively low mechanical strength, exhibits time-dependant deformation properties. The rich natural, or induced, pore and micro-crack behaviour of porous sandstone created the conditions for volumetric creep. Triaxial creep tests under different stress conditions were conducted to investigate the time-dependant deformation properties of porous sandstone. The sandstone samples used in triaxial creep tests were prepared by following the same specification as the triaxial compressive tests in Section 3.2.

2.3.1. Time-dependant deformation of porous sandstone under different confining pressure

To analyse the time-dependant deformation of porous sandstone under a hydrostatic stress state, confining pressure shown was applied incrementally to the specimens at 5, 10, 20, and 30 MPa. The temperature was set to a constant 25 °C. And the temperature fluctuation was controlled in range of ±0.1 °C. In order to measure the displacement in the radial and axial directions, the toroidal deformation metre and LVDT displacement sensor were used in the triaxial creep tests. And the toroidal deformation metre is mainly made of spring steels and resistor strain gage. The calibration result of toroidal deformation metre and LVDT displacement sensor provide their linearity are respectively 0.35% and 0.18%, as well as the linear range of ±1 mm and ±5 mm, respectively. Furthermore, the axial displacement ΔL and lateral displacement ΔD are both accurate to 10^{-4} mm. On the basis of the axial strain ε_1 and lateral strain ε_3, the volumetric strain e_{vol} is figured out by summed up the twice lateral strain and the axial strain, i.e. $e_{vol} = \varepsilon_1 + 2\varepsilon_3$. For the sandstone specimen under hydrostatic pressure of 5, 10, 20 and 30 MPa, the volumetric strain versus time curve at each confining pressure is shown in Fig. 3.

Table 1
Compressive strength of porous sandstone samples under different confining pressure.

Confining pressure (MPa)	Compressive strength (MPa)			
	Sample 1	Sample 2	Sample 3	Average value
5	25.18	26.01	25.94	25.71
10	37.89	38.33	37.82	38.01
15	48.39	48.10	48.05	48.18
20	52.77	52.77	53.10	53.01
30	71.60	70.96	71.27	71.28

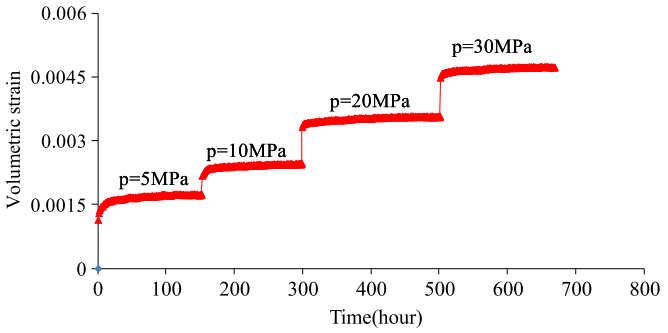

Fig. 3. Volumetric creep curve of a sandstone specimen under different hydrostatic pressure: 5, 10, 20, and 30 MPa.

In Fig. 3, the volumetric strain in a sandstone specimen increased and gradually stabilized with time at load level. With increased load, the increment of volume strain with time gradually slowed thus showing the volumetric creep properties of porous sandstone.

2.3.2. Time-dependant deformation of porous sandstone under different deviatoric stress

Multi-step deviatoric stress was applied to a sandstone sample at the same confining pressure to study the creep behaviour of porous sandstone. In the triaxial creep test, the confining pressure was increased to 6 MPa and then the axial deviatoric stress increased incrementally to 12, 14, 16, and 18 MPa. The axial strain versus time curve is shown in Fig. 4.

2.3.3. Comparison of test results under hydrostatic and non-hydrostatic stress states

On the basis of continuum mechanics, the stress tensor σ_{ij} is decomposed into two parts: the mean stress tensor σ_m and the stress deviator tensor s_{ij}, i.e., $\sigma_m = \sigma_{ii}/3$ and $\sigma_{ij} = \sigma_m\delta_{ij} + s_{ij}$. In the same way, the strain tensor ε_{ij} is divided into a mean part e_{vol} associated with a change in volume and a deviatoric part e_{ij} associated with a change in shape (distortion), i.e., $\varepsilon_{ij} = (e_{vol}/3)\delta_{ij} + e_{ij}$.

Comparing the loading path of the triaxial creep tests in Section 2.3.1 and 2.3.2, the former applied confining pressure only, i.e., the hydrostatic stress state, while the latter saw the superposition of confining stress and deviatoric stress, i.e., a non-hydrostatic state. To analyse the time-dependant deformation of porous sandstone samples under hydrostatic and non-hydrostatic stress states, the second loading level of hydrostatic stress state in Fig. 3 and the

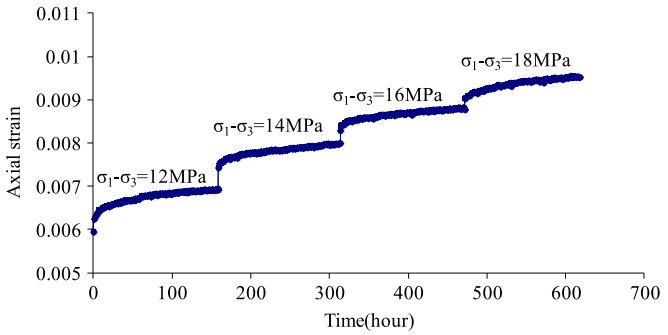

Fig. 4. Axial creep curve: sandstone under multi-stage deviatoric compression (12, 14, 16, and 18 MPa) at constant confining pressure of 6 MPa.

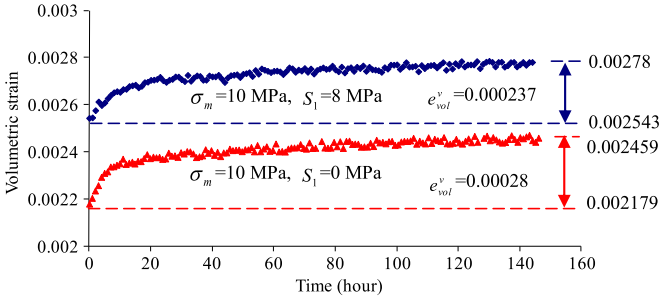

Fig. 5. Volumetric creep curve: sandstone specimens under the same mean stress of 10 MPa and different deviatoric component: $S_1=0$ MPa and $S_1=8$ MPa.

first loading level of non-hydrostatic stress state in Fig. 4 were compared as shown in Fig. 5. And this choice of loading levels ensures that the comparison analysis has the same mean stress, $\sigma_m=10$ MPa and different stress deviator tensor, i.e., the former had no deviatoric component and the latter had a deviatoric component,

$$s_{ij}=\begin{bmatrix} S_1 & 0 & 0 \\ 0 & S_2 & 0 \\ 0 & 0 & S_3 \end{bmatrix}=\begin{bmatrix} 8 & 0 & 0 \\ 0 & -4 & 0 \\ 0 & 0 & -4 \end{bmatrix} \quad (1)$$

In Fig. 5, the red triangles represented the volumetric creep curve under hydrostatic stress ($\sigma_m=10$ MPa, $S_1=0$ MPa) and the blue squares represented the volumetric creep curve under a non-hydrostatic stress state ($\sigma_m=10$ MPa, $S_1=8$ MPa). The viscous volumetric strain e^v_{vol} was calculated by subtracting the instantaneous elastic volumetric strain e^e_{vol} from the total volumetric strain e_{vol}. After about 145 h, the two creep curves reached a stable state, such that the axial deformation rate was below 10^{-10}/s.[25] Table 1 lists the strains and the proportion of viscous volumetric strain at stable creep states in the total volumetric strain.

From Fig. 5 and Table 2, porous sandstone sample exhibited viscous volumetric deformation under hydrostatic and non-hydrostatic stress states: the proportion of viscous volumetric strain at a stable creep state in the total strain was approximately 10%. That means the compaction of porous sandstone under the above stress condition is time-dependant. To analyse the contribution of different stress components (hydrostatic and deviatoric) on viscous volumetric strain, the first loading level of non-hydrostatic stress state in Fig. 4 was taken as an example and the axial viscous strain ε_1^v calculated by subtracting the instantaneous elastic axial ε_1^e strain from the total axial strain ε_1, i.e. $\varepsilon_1^v=\varepsilon_1-\varepsilon_1^e$.

In Fig. 6, the blue triangles represented the axial viscous strain ε_1^v and the red squares represented one-third of the viscous volumetric strain e^v_{vol}, which indicated the contribution of volumetric creep to time-dependant axial strain, *i.e.*, $\varepsilon_1^v=(1/3)e^v_{vol}+e_1^v$. According to the strain tensor in continuum mechanics, volumetric strain depends on mean stress (hydrostatic stress state) while the distortion strain arises because of the deviatoric stress tensor.

Table 2
Volumetric strain, viscous volumetric strain, and viscous strain proportion for porous sandstone samples under hydrostatic and non-hydrostatic stress states.

Stress state	Instantaneous elastic volumetric strain	Stable volumetric strain	Viscous volumetric strain	Viscous strain proportion (%)
$\sigma_m=10$ MPa, $S_1=0$ MPa	0.00218	0.00246	0.00028	11.4
$\sigma_m=10$ MPa, $S_1=8$ MPa	0.00254	0.00278	0.00024	8.6

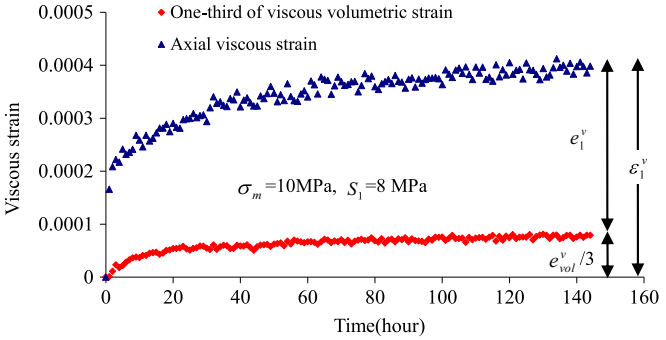

Fig. 6. The axial viscous strain and the one-third of viscous volumetric strain versus time for the sandstone specimens under the mean stress of 10 MPa and axial stress deviator of 8 MPa.

Therefore, the different value between these two curves meant that the viscous strain in the axial direction was caused by the deviatoric stress component. In Fig. 6, the contribution of volumetric creep to axial viscous strain amounted to about 20% of the total axial viscous strain. For porous sandstone the viscous volumetric strain should not be neglected.

3. Creep model for porous sandstone

On the basis of the experimental results, time-dependant volumetric strain should be considered in the deformation mechanism of porous sandstone. However, previous creep models, such as Burger's model and Burgers-creep visco-plastic model, ignore the viscous volumetric behaviour which is negligible for relatively compact geologic materials but not for porous rock. The Burgers model is characterised by visco-elastic deviatoric behaviour and an elastic volumetric component, while the Burgers-creep visco-plastic model has an added plastic dimension to these two behaviours.[19]

To reveal the viscous volumetric behaviour in a creep model for porous sandstone, Burger's model (a Kelvin cell in series with a Maxwell component) was modified by the addition of a volumetric creep component to describe the visco-elastic deviatoric behaviour and visco-elastic volumetric behaviour (see Fig. 7).

In Fig. 7, K^M and K^K are the bulk modulus of spring elements in the Maxwell and Kelvin components, respectively, G^M and G^K are the shear modulus of the spring elements in the Maxwell and Kelvin components, respectively, η_m^M and η_m^K are the volumetric viscosity coefficients of dashpot elements in the Maxwell and Kelvin components respectively, and η_s^M and η_s^K are the deviatoric viscosity coefficients of the dashpot elements in the Maxwell and

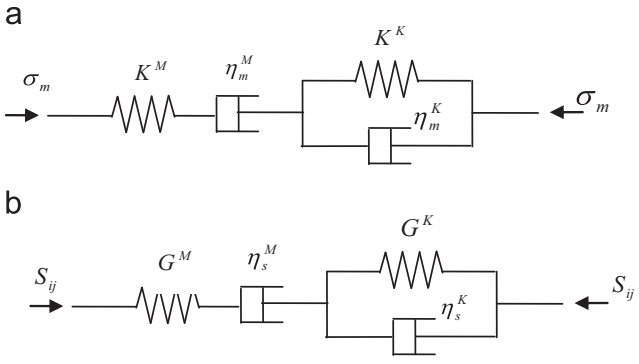

Fig. 7. Schematic representation of the modified Burgers model (a) volumetric behaviour and (b) deviatoric behaviour.

Kelvin components respectively.

3.1. Visco-elastic constitutive law for volumetric behaviour

According to the schematic representation of the modified Burgers model in Fig. 7(a), its volumetric behaviour is extended to a three-dimensional formulation. With reference to Hooke's law for spherical stress states $\sigma_m = K\varepsilon_v$ in elastic mechanics, its differential form is:

$$P''(D)\sigma_m = Q``(D)\varepsilon_v \tag{2}$$

where $P''(D) = \sum_{k=0}^{l} p_k'' \partial^k(\cdot)/\partial t^k$, $Q``(D) = \sum_{k=0}^{r} q_k^{``} \partial^k(\cdot)/\partial t^k$, and $D = \partial(\cdot)/\partial t$ is the differential operator in real-time domain.

Ignoring time-dependant volumetric deformation, the differential operator on both sides was constant, i.e. $P''(D) = 1$; $Q''(D) = K$. While the volumetric viscous deformation was taken into consideration, its three-dimensional constitutive relation under spherical stress states was obtained by Laplace transformation of both sides of Eq. (2):

$$\sigma_m + \left(\frac{\eta_m^M}{K^M} + \frac{\eta_m^M + \eta_m^K}{K^K}\right)\dot{\sigma}_m + \frac{\eta_m^M \eta_m^K}{K^M K^K}\ddot{\sigma}_m = \eta_m^M \dot{e}_{vol} + \frac{\eta_m^M \eta_m^K}{K^K}\ddot{e}_{vol} \tag{3}$$

where $\dot{\sigma}_m$ and $\ddot{\sigma}_m$ are the first and second derivative of the average stress, respectively; $\dot{e}_{vol}$ and $\ddot{e}_{vol}$ are the first and second derivatives of the volumetric strain, respectively.

3.2. Visco-elastic constitutive law for deviatoric behaviour

According to the schematic representation of deviatoric behaviour in the visco-elastic constitutive model in Fig. 7(b), the Laplace form of differential constitutive model for deviatoric stress is expressed with reference to Hooke's law, $S_{ij} = 2Ge_{ij}$, as follows:

$$P'(D)S_{ij} = 2Q'(D)e_{ij} \tag{4}$$

The three-dimensional constitutive relationship under deviatoric stress is:

$$S_{ij} + \left(\frac{\eta_s^M}{G^M} + \frac{\eta_s^M + \eta_s^K}{G^K}\right)\dot{S}_{ij} + \frac{\eta_s^M \eta_s^K}{G^M G^K}\ddot{S}_{ij} = 2\eta_s^M \dot{e}_{ij} + \frac{2\eta_s^M \eta_s^K}{G^K}\ddot{e}_{ij} \tag{5}$$

where $\dot{S}_{ij}$ and $\ddot{S}_{ij}$ are the first and second derivatives of deviatoric stress tensor, respectively; $\dot{e}_{ij}$ and $\ddot{e}_{ij}$ are the first and second derivatives of the deviatoric strain tensor, respectively.

3.3. Three-dimensional creep constitutive model of porous sandstone

As Fig. 7 shows, the creep model for porous sandstone consisted of a Maxwell component and a Kelvin component. The time-dependant volumetric strain equation under a spherical stress state was expressed in a similar format to the deviatoric stress state in which the shear modulus and shear viscous coefficient were replaced by a volumetric modulus and volumetric viscous coefficient. According to $\varepsilon_{ij}(t) = (1/3)e_{vol}(t)\delta_{ij} + e_{ij}(t)$, the total time-dependant strain is given by:

$$\varepsilon_{ij}(t) = \left(\frac{\sigma_m}{3K^M} + \frac{\sigma_m}{3\eta_m^M}t + \frac{\sigma_m}{3K^K}\left(1 - e^{-\frac{K^K}{\eta_m^K}t}\right)\right)\delta_{ij} + \frac{S_{ij}}{2G^M} + \frac{S_{ij}}{2\eta_s^M}t + \frac{S_{ij}}{2G^K}\left(1 - e^{-\frac{G^K}{\eta_s^K}t}\right) \tag{6}$$

4. Numerical simulation of the creep model for porous sandstone

To reveal the creep behaviour of porous sandstone by a numerical approach, the finite difference method was used to express the modified Burgers model in Section 3. Furthermore, the creep model was programmed in FLAC3D to simulate the creep behaviour of porous sandstone samples under hydrostatic and non-hydrostatic stress states. The sandstone sample (a 50 mm diameter, 100 mm high cylinder) was divided into 1000 elements and 1111 nodes and its base given a boundary condition on zero *Y*-direction displacement.

4.1. Determination of model parameters

The classification of model parameters in the creep model for porous sandstone is listed in Table 3. K^M, K^K, η_m^M and η_m^K are used to describe the volumetric behaviour, while G^M, G^K, η_s^M, and η_s^K are used for deviatoric behaviour. K^M and G^M could be obtained by substituting the initial volumetric strain, the initial axial deviatoric strain, the mean stress and the axial deviatoric stress into the component formulae for the initial condition.

According to the volumetric creep curve and the axial deviatoric creep curve, volumetric parameters K^K, η_m^M, η_m^K and deviatoric parameters G^K, η_s^M, η_s^K are respectively deduced by establishing an objective function and minimising the difference between calculated and measured values.

4.2. Numerical simulation of creep model for porous sandstone under hydrostatic stress

According to the volumetric creep curve under hydrostatic pressure in Section 2.3.1, the creep parameters at each pressure were calculated by the method outlined in Section 4.1 (Table 4). The simulated results from the creep model are compared to the measured creep test data in the form of volumetric creep curves (see Fig. 8).

4.3. Numerical simulation of the creep model for porous sandstone under non-hydrostatic stress

For non-hydrostatic stress states, the creep deformation of four sandstone samples under different stresses (Table 5) were simulated and compared with the measured results. These four samples were subjected to the same mean stress and different

Table 3
Classification of creep model parameters for porous sandstone.

Behaviour	Kelvin component	Maxwell component
Volumetric	K^K, η_m^K	K^M, η_m^M
Deviatoric	G^K, η_s^K	G^M, η_s^M

Table 4
Creep parameters under hydrostatic pressure.

σ_m (MPa)	K^M (GPa)	K^K (GPa)	η_m^M (GPa h)	η_m^K (GPa h)
5	4.4	10.4	5680	55.3
10	4.6	50.9	15,823	267.5
20	6.0	185.0	22,520	493.7
30	6.7	216.6	35,510	767.0

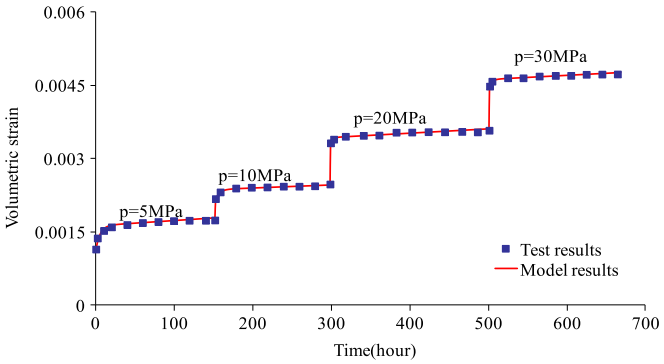

Fig. 8. Comparison of simulated and measured volumetric creep curves for sandstone samples.

Table 5
Different stress state for four sandstone samples.

No.	Confining pressure σ_3 (MPa)	Deviatoric stress $\sigma_1-\sigma_3$ (MPa)	Mean stress σ_m (MPa)	Axial deviator stress S_1 (MPa)
1	5	12	9	8
2	6	9	9	6
3	7	6	9	4
4	8	3	9	2

Table 6
Model parameters for sandstone samples under different confining pressures and different axial deviatoric stress.

No.	K^M (GPa)	G^M (GPa)	K^K (GPa)	G^K (GPa)	η_m^M (GPa h)	η_s^M (GPa h)	η_m^K (GPa h)	η_s^K (GPa h)
1	1.51	0.789	22.68	5.35	9897	3534	353	85.8
2	1.56	0.794	19.56	7.05	8386	12,299	304	89.6
3	1.58	0.830	19.08	13.65	7802	26,017	283	136
4	1.60	0.838	17.67	18.95	5302	62,589	16	143

deviatoric stresses, and are arranged in increasing order. According to Section 4.1, the model parameters of four sandstone samples under different stresses were listed in Table 6. The model and test axial strain data for these sandstone samples were shown in Fig. 9. Regardless of the time-dependant volumetric strain, the model creep curve degraded (Fig. 9) to Burgers model, with the same parameters as Table 6, i.e., K^M, G^M, G^K, η_s^M, and η_s^K.

In Fig. 9, due to the application of the volumetric viscosity coefficient, the modified model results were a better fitting to the experimental data than the Burgers model. The Burgers model, neglecting the viscous volumetric behaviour, underestimated the strain in the porous sandstone: the proportion of the difference in values was underestimated by the Burgers model when the axial viscous strain increased with an increasing ratio of mean stress with respect to axial deviator stress.

The evolution of model parameters for sandstone samples under different stresses are shown in Fig. 10. Comparing the variations in these parameters, three conclusions were drawn: firstly the elastic parameters, including bulk modulus K^M and shear modulus G^M, increased with the confining pressure. The increasing consolidation effect of the confining pressure on porous sandstone can be accounted for by the associated increases in the elastic deformation parameters. The more compacts the material, the harder it was to deform. Secondly, the parameters with respect to volumetric viscous behaviour, such as bulk modulus K^K and viscosity coefficient η_m^M and η_m^K, decreased with increasing confining pressure. Although the mean stress on the four samples was the same, their parameters with respect to volumetric viscous

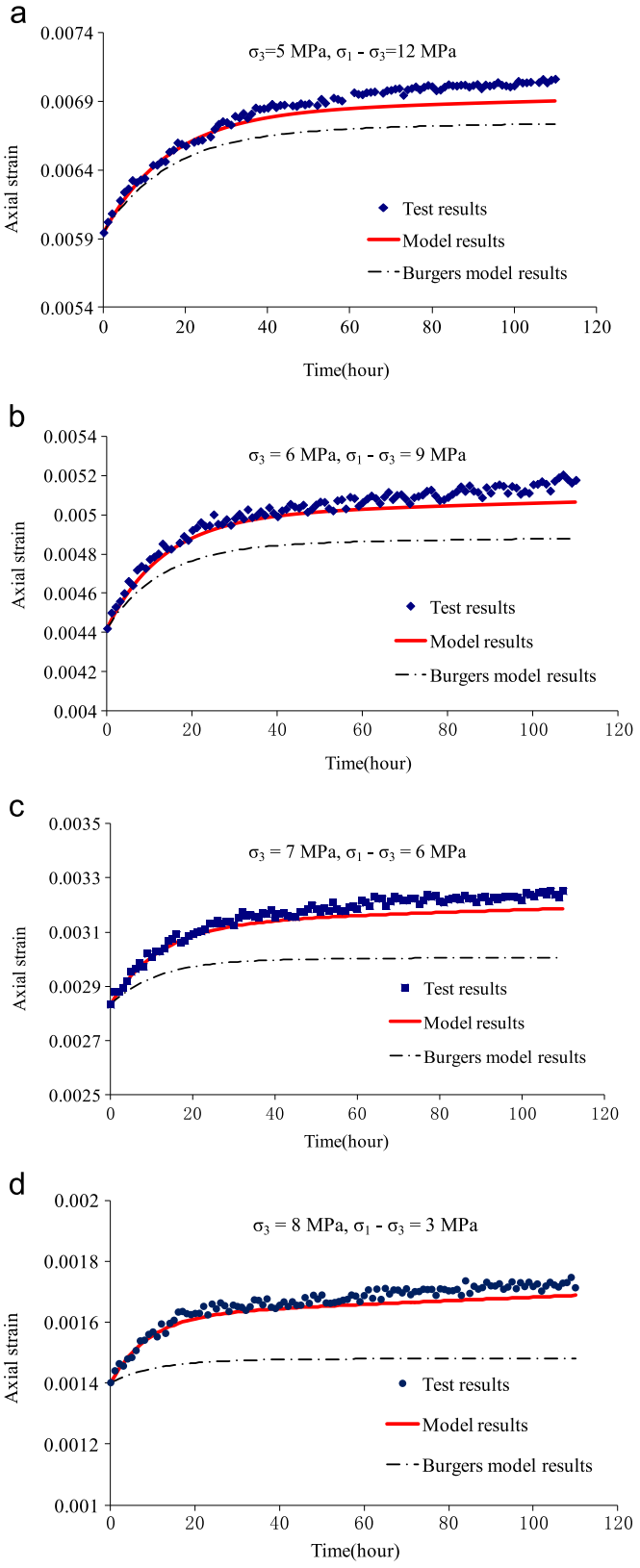

Fig. 9. Comparison of test results, model results, and Burger's model results: axial strain in sandstone samples. (a) σ_3=5 MPa, $\sigma_1-\sigma_3$=12 MPa; (b) σ_3=6 MPa, $\sigma_1-\sigma_3$=9 MPa; (c) σ_3=7 MPa, $\sigma_1-\sigma_3$=6 MPa; (d) σ_3=8 MPa, $\sigma_1-\sigma_3$=3 MPa.

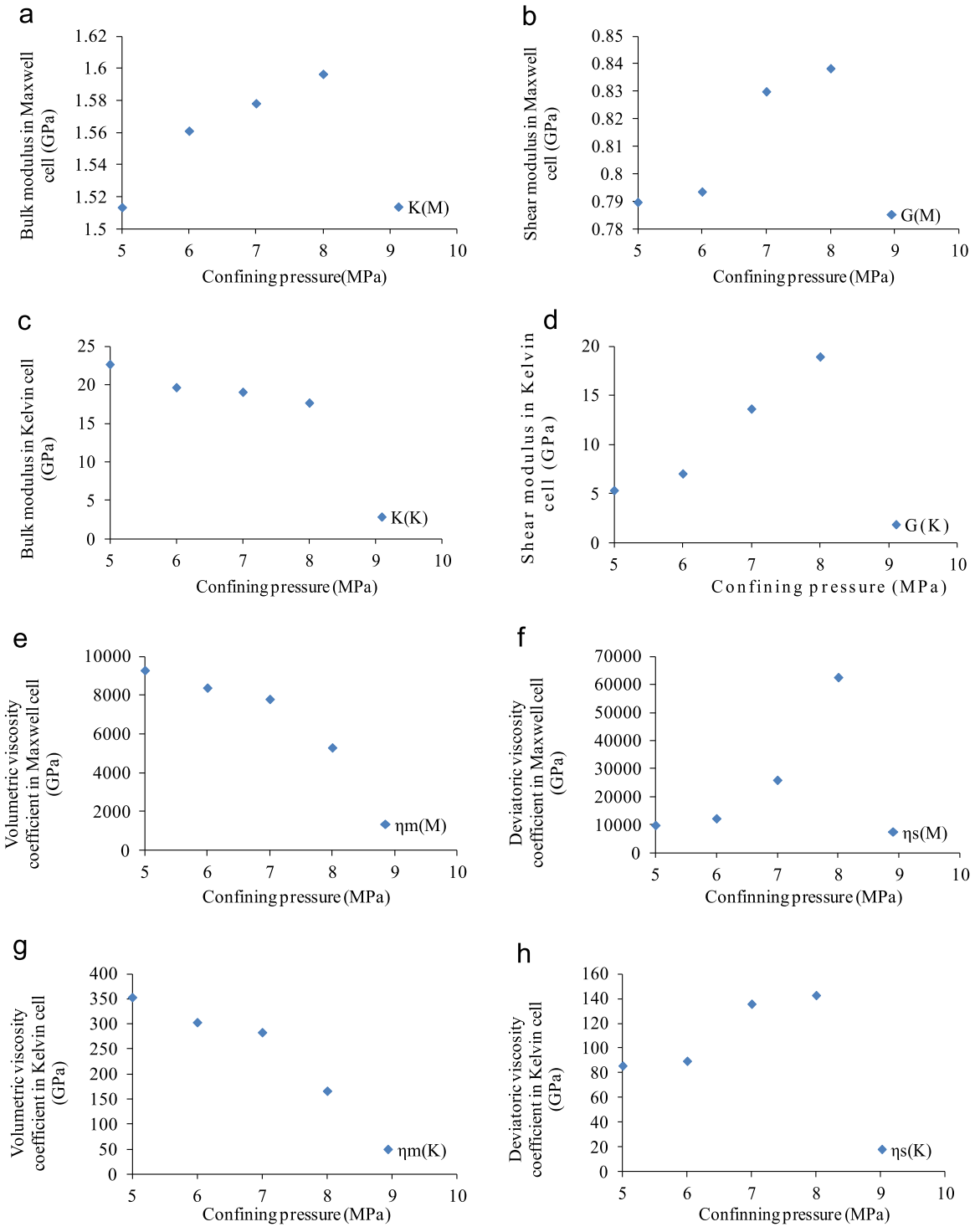

Fig. 10. The evolution of (a) bulk modulus in the Maxwell cell, (b) shear modulus in the Maxwell cell, (c) bulk modulus in the Kelvin cell, (d) shear modulus in the Kelvin cell, (e) volumetric viscosity coefficient in the Maxwell cell, (f) deviatoric viscosity coefficient in the Maxwell cell, (g) volumetric viscosity coefficient in the Kelvin cell and (h) deviatoric viscosity coefficient in the Kelvin cell for sandstone samples under different stresses.

behaviour varied. Thirdly, the parameters with respect to deviatoric viscous behaviour, such as shear modulus $G^K$and viscosity coefficients η_s^M and η_s^K, increased with the incremental confining pressure or the diminution of deviatoric stress.

5. Discussion

The proposed creep model was intended to describe the visco-elastic deformation behaviour of porous sandstone. If the time-dependant volumetric deformation in Section 3.1 was ignored, the creep model for porous sandstone in Eq. (6) reduces to the Burgers model, i.e.,

$$\varepsilon_{ij}(t) = \left(\frac{\sigma_m}{3K^M}\right)\delta_{ij} + \frac{S_{ij}}{2G^M} + \frac{S_{ij}}{2\eta_s^M}t + \frac{S_{ij}}{2G^K}\left(1 - e^{-\frac{G^K}{\eta_s^K}t}\right) \tag{7}$$

This model was not confined to visco-elastic problems: the creep model could be transplanted into other models. For

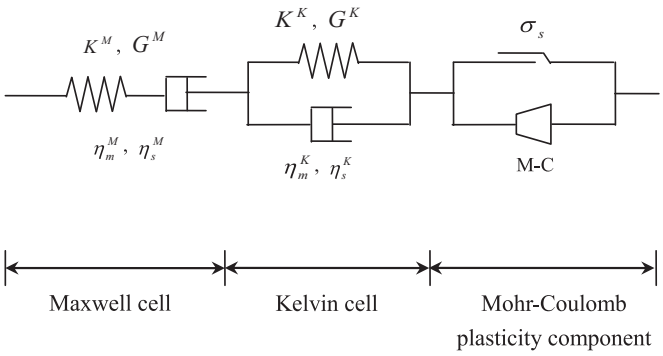

Fig. 11. Schematic representation of the modified Burgers-creep visco-plastic model.

example, since the Burgers-creep visco-plastic model consisted of a Burgers model and a Mohr–Coulomb plasticity model, it could be characterised by a visco-elasto-plastic deviatoric behaviour and a visco-elasto-plastic volumetric behaviour by replacing the Burgers model with the modified one (Fig. 11).

In this way, the proposed creep model for porous sandstone was extended from visco-elastic to visco-elasto-plastic. Before reaching its plastic yielding phase, the sandstone was visco-elastic. In Fig. 11, the visco-elasto-plasticity constitutive relationships of the creep model comprise the Maxwell component, Kelvin component, and Mohr–Coulomb plasticity component.

6. Conclusions

The long-term deformation behaviour of porous sandstone has been investigated using laboratory tests and theoretical analysis. A series of laboratory test including triaxial compressive tests and creep tests were conducted. Comparing the time-dependant deformation of porous sandstone under different stress components, the results indicated that porous sandstone, under both hydrostatic and non-hydrostatic stress states, exhibited viscous volumetric behaviour. The contribution of volumetric creep to axial viscous strain amounted to approximately 20% of the total axial viscous strain, which meant that the viscous volumetric deformation of porous sandstone was non-ignorable.

Porous sandstone, as a compressible material, demonstrated diverse creep behaviours under different stress components: volumetric creep under spherical stress and shear creep under deviatoric stress. As a result of the non-ignorable viscous volumetric deformation in porous sandstone, the Burgers model was modified by using volumetric viscosity parametersK^K, η_m^M, and η_m^K. On that basis, the creep model was established with two stress component. In the creep model for porous sandstone, the bulk modulus and volumetric viscosity coefficient were applied as visco-elastic parameters pertaining to the spherical stress component, while shear modulus and deviatoric viscosity coefficient were used to model the behaviour under deviatoric stress. In this way, the modified model for porous sandstone catered for visco-elastic deviatoric behaviour and visco-elastic volumetric behaviour.

Moreover, through the numerical example of the modelling of the porous sandstone samples, the model was shown to have been able to simulate the time-dependant deformation of porous sandstone by comparing the output of the model to test data. The agreement between the output from the creep model and the test results was better than that from the Burgers model: the larger the ratio of mean stress to axial deviator stress, the closer their agreement. The difference between the output from the creep model and the test results gradually increased with the reduction of the ratio of mean stress to axial deviator stress. This might have been due to the visco-elastic model not considering plastic deformation or the hypothesis that there was no contribution of deviatoric stress component to volumetric creep. Therefore, the modified Burgers-creep viscous-plastic model should be taken into consideration for the analysis of the deformation of sandstone under high deviatoric stresses in future studies. Furthermore, the interaction between volumetric creep under the spherical stress component and shear creep under the deviatoric stress component should be included in further research.

This creep model was used for the analysis of the skeleton of a porous rock mass, such as porous sandstone, which underwent time-dependant volumetric deformation. When considering the ground water conditions, the stress should be replaced by the effective stress, especially in reservoir engineering applications. The long-term extraction or injection of underground water, oil, or gas changed the pore pressure in the aquifer which affected the effective stress and deformation of the sandstone skeleton. Besides modelling deformation behaviour of reservoir skeletons, its hydraulic behaviour modelling capabilities are also of interest to civil engineers. This creep model for porous sandstone can not only provide a theoretical model for the time-dependant deformation of a reservoir skeleton, but also can describe the creep characteristics of compressible porous materials to further improve the rheological modelling of geological materials.

Acknowledgement

This paper is financially supported by National Natural Science Foundation of China under Grant no. 50920105908. Authors would like to thank useful comments of reviewer and editors for improving the manuscript.

References

[1] Zimmerman RW, Somerton WH, King MS. Compressibility of porous rocks. J Geophys Res 1986;91:12765–77.
[2] Rice JR, Cleary MP. Some basic stress diffusion solutions for fluid saturated elastic porous media with compressible constituents. Rev Geophys 1976;14:227–41.
[3] Lu YF, Tian B, Zhou SP, Shao JF. Laboratory and theoretical on sandstone. Chin J Rock Mech Eng 2005;24(18):3360–7.
[4] Lydzba D, Pietruszczak S, Shao JF. Intergranular pressure solution in chalk: a multiscale approach. Comput Geotech 2007;34(4):291–305.
[5] He W, Hajash A, Sparks D. A model for porosity evolution during creep compaction of sandstones. Earth Planet Sci Lett 2002;197(3):237–44.
[6] Geertsma J. Land subsidence above compacting oil and gas reservoirs. J Can Petrol Technol 1973;25(6):734–44.
[7] Nguyen VH, Gland N, Dautriat J, et al. Compaction, permeability evolution and stress path effects in unconsolidated sand and weakly consolidated sandstone. Int J Rock Mech Min Sci 2014;67:226–39.
[8] Michael K, Bunch M, Varma S. Simulation of the cumulative impacts of CO_2 geological storage and petroleum production on aquifer pressures in the offshore Gippsland Basin. Int J Greenh Gas Control 2013;19:310–21.
[9] Liteanu E, Spiers CJ. Influence of pore fluid salt content on compaction creep of calcite aggregates in the presence of supercritical CO_2. Chem Geol 2009;265(1):134–47.
[10] Xiao X, Evans B. Shear-enhanced compaction during non-linear viscous creep of porous calcite–quartz aggregates. Earth Planet Sci Lett 2003;216(4):725–40.
[11] Fokker PA, Visser K, Peters E, et al. Inversion of surface subsidence data to quantify reservoir compartmentalization: A field study. J Petrol Sci Eng 2012;96:10–21.
[12] Fielding EJ, Blom RG, Goldstein RM. Rapid subsidence over oil fields measured by SAR interferometry. Geophys Res Lett 1998;25(17):3215–8.
[13] Pacheco-Martínez J, Hernandez-Marin M, Burbey TJ, et al. Land subsidence and ground failure associated to groundwater exploitation in the Aguascalientes Valley, Mexico. Eng Geol 2013;164:172–86.
[14] Ito H, Sasajima S. A ten year creep experiment on small rock specimens. Int J Rock Mech Min Sci 1987;24(2):113–21.
[15] Ito H. The phenomenon and examples of rock creep. In: Hudson JH, editor. Comprehensive Rock Engineering, vol. 3. Oxford: Pergamon Press; 1993. p. 693–708.

[16] Challamel N, Lanos C, Casandjian C. Creep damage modelling for quasi-brittle materials. Eur J Mech A 2005;24(4):593–613.
[17] Darabi MK, Abu Al-Rub RK, Masad EA, Huang CW, Little DN. A thermo–viscoelastic–viscoplastic–visco damage constitutive model for asphaltic materials. Int J Solids Struct 2011;48(1):191–207.
[18] Abu Al-Rub RK, Darabi MK. A thermodynamic framework for constitutive modeling of time- and rate-dependent materials. Part I: Theory. Int J Plasticity 2012;34:61–92.
[19] Sharifzadeh M, Tarifard A, Moridi MA. Time-dependent behavior of tunnel lining in weak rock mass based on displacement back analysis method. Tunn Under Space Tech 2013;38:348–56.
[20] Fahimifar A, Tehrani FM, Hedayat A, Vakilzadeh A. Analytical solution for the excavation of circular tunnels in a visco-elastic Burger's material under hydrostatic stress field. Tunn Under Space Tech 2010;25(4):297–304.
[21] Boidy E, Bouvard A, Pellet F. Back analysis of time-dependent behavior of a test gallery in claystone. Tunn Under Space Tech 2002;17(4):415–24.
[22] Pellet F. Contact between a tunnel lining and a damage-susceptible viscoplastic medium. Comp Model Eng Sci 2009;52(3):279–96.
[23] Dahou A, Shao JF, Bederiat M. Experimental and numerical investigations on transient creep of porous chalk. Mech Mater 1995;21(2):147–58.
[24] Wang ZY, Li YP. Rock Rheological Mechanics and Numerical Simulation. 1st ed.. Beijing: Science Press; 2008.
[25] Jun S. Rheological Behavior of Geomaterial and its Engineering Application. 1st ed.. Beijing: China Architecture and Building; 1999.